Nanoscale

PAPER

View Article Online
View Journal | View Issue

Cite this: *Nanoscale*, 2019, **11**, 3993

Prediction of MXene based 2D tunable band gap semiconductors: GW quasiparticle calculations

Yujuan Zhang, †[a,b] Weiyi Xia,†[b] Yabei Wu[b,c] and Peihong Zhang *[b,c,d]

Received 6th February 2019,
Accepted 9th February 2019

DOI: 10.1039/c9nr01160a

rsc.li/nanoscale

MXenes are a large family of layered transition metal carbide/nitride materials that possess a number of desired properties such as flexible chemical composition, high mechanical strength, and excellent structural stability. Although MXene based semiconductors have attracted considerable recent research attention in the search of novel 2D electronic materials, accurate understanding of their electronic properties has not been established. In this work, we carry out fully converged GW quasiparticle calculations for M_2CO_2 (M = Hf, Zr, and Ti) MXene based 2D semiconductors and alloys using newly developed accelerated GW methods. The quasiparticle band gaps of single-layer Hf_2CO_2, Zr_2CO_2, and Ti_2CO_2 are predicted to be 2.45, 2.13, and 1.15 eV, respectively. The narrow band gap of Ti_2CO_2 is attributed to the low energy of Ti 3d as compared with the Hf and Zr d states. Considering their chemical similarity, it is expected that $Hf_{2-2x}Ti_{2x}CO_2$ semiconductors can be synthesized without difficulties. We show that the quasiparticle band gap of $Hf_{2-2x}Ti_{2x}CO_2$ ($0 \le x \le 1$) semiconductor alloy can be continuously tuned from 2.45 to 1.15 eV, offering a unique 2D semiconductor with a moderate and tunable gap for future electronics applications.

1. Introduction

MsXenes are a new family of layered transition metal carbide/nitride materials which have attracted considerable research interest since nanosheets of Ti_3C_2 MXene were first synthesized.[1–4] MXenes can be synthesized by exfoliating the "A" laminar component from the MAX matrix phase in HF solution at low temperature. The MAX phase has a general chemical formula $M_{n+1}AX_n$ (n = 1, 2, or 3), where M is an early transition metal (M = Sc, Ti, V, Cr, Zr, Nb, Mo, Hf, Ta or W), A is a Group IIIA or IVA element (A = Al, Ga, In, Si, Ge, Sn, Pb, P, As, S or Cd) and X is C and/or N.[5] The strong M–X bonds have a mixed ionic, metallic and covalent character, while the M–A bond shows typical metallic nature. The disparate bonding strength among the M–A and M–X bonds in the MAX phase makes it possible to selectively etch out the A layers without disrupting the M–X framework. Since the as-synthesized MXenes are typically terminated by O, OH and/or F groups, they are usually denoted as $M_{n+1}X_nT_x$ (n = 1, 2, and 3), with T standing for the terminating groups. MXenes combine the advantages of metals and ceramics, exhibiting high chemical stability, excellent electrical conductivity and exceptional mechanical properties. A number of potential applications have been proposed for these emerging layered materials, including Li-batteries,[6–8] highly conductive optical coating,[9] high volumetric capacitors,[10] and hydrogen storage.[11]

Most MXenes are metallic, but there are also a number of MXene semiconductors reported. For example, Hf_2CO_2, Zr_2CO_2, V_2CF_2, $V_2C(OH)_2$, Ti_2CO_2, $Sc_2C(OH)_2$, Sc_2CF_2 and Sc_2CO_2 are found to possess nonzero band gaps.[7,8,12,13] These layered semiconductors may have some of the most sought-after properties such as having a moderate band gap and being highly stable, among others, opening a new avenue for fabricating next generation 2D electronic devices. For example, Hf_2CO_2 has been shown[14] to have a higher thermal conductivity than that of the much studied phosphorene or MoS_2, and a high carrier mobility comparable to that of phosphorene. The reported band gap of single-layer (which consists of five atomic layers as shown in Fig. 1) Hf_2CO_2 MXene is 1.65 eV (ref. 14) using the Heyd–Scuseria–Ernzerhof (HSE) hybrid functional[15,16] within density functional theory (DFT).

Although the HSE functional has been shown to be able to predict the band gap of a wide range of bulk semiconductors with reasonable accuracy, there are notable exceptions. For example, the measured band gap of FeS_2 is about 0.95 eV,[17]

[a]*School of Materials Science and Engineering, University of Science and Technology Beijing, Beijing 100083, China*
[b]*Department of Physics, University at Buffalo, State University of New York, Buffalo, New York 14260, USA*
[c]*International Centre for Quantum and Molecular Structures and Department of Physics, Shanghai University, Shanghai 200444, China*
[d]*Beijing Computational Science Research Center, Beijing 100084, China.*
E-mail: pzhang3@buffalo.edu
†Y. Z. and W. X. contributed equally to this work.

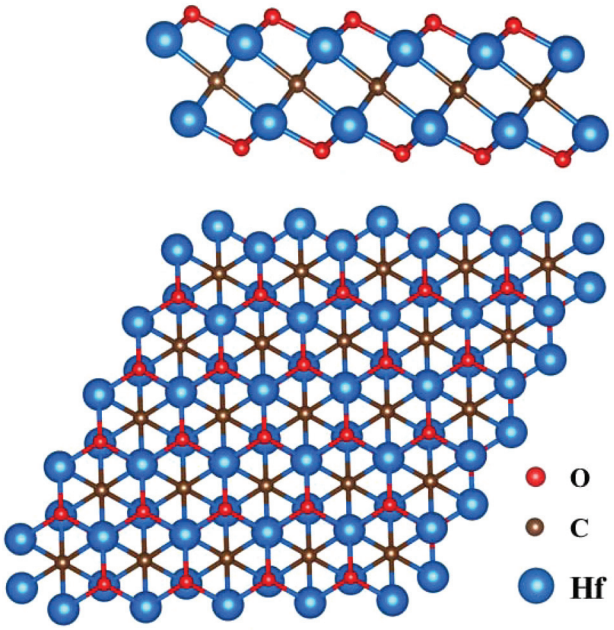

Fig. 1 Side view (upper) and top view (lower) of the crystal structure of single layer Hf_2CO_2.

but the HSE functional predicts a band gap of FeS_2 of about 2.7 eV. In addition, straightforward applications of the HSE functional to predict the quasiparticle band gap of 2D materials deserve scrutiny since the dielectric screening properties in 2D materials are fundamentally different from those in bulk materials. A more rigorous approach for calculating the band gap, and more generally, the quasiparticle band structure, of semiconductors is the GW method.[18] Therefore, it is imperative to carry out GW calculations for these emerging 2D semiconductors.

In this work, we have carried out first-principles quasiparticle calculations for Hf_2CO_2 within the GW approximation[18] using a local version of the BERKELEYGW package.[19] We find that the GW band gap of monolayer Hf_2CO_2 is about 2.45 eV. This value is significantly larger than the value (1.65 eV) predicted by the HSE functional. Since the optimal band gap of semiconductors varies significantly from applications to applications, for example, narrow gap semiconductors may be suitable for infrared or thermoelectric applications whereas power electronics requires wide-gap semiconductors, it is often desirable that the band gap of a class of materials (*e.g.*, 2D MXenes in this work) be tunable to suit different applications. Considering the chemical flexibility of MXenes, it is likely that their band gap can be conveniently tuned through chemical substitutions of the metallic sites with isoelectronic elements. To this end, we have also carried out DFT and GW calculations for single-layer Zr_2CO_2, Ti_2CO_2 and $Hf_{2-x}Ti_xCO_2$. We find that the quasiparticle band gap of $Hf_{2-x}Ti_xCO_2$ can be continuously tuned from 2.45 to 1.15 eV with increasing Ti concentration, offering a promising material system for a wide range of applications.

2. Computational details

Structural optimizations and DFT band structure calculations are carried out using the Vienna *ab initio* simulation package (VASP).[20] The interaction between valence electrons and the ionic cores is described using the projector augmented wave (PAW) approach.[21] The generalized gradient approximation (GGA)[22] functional of Perdew–Burke–Ernzerhof (PBE)[23] is used for DFT calculations. A relatively high cutoff energy of 500 eV for the plane-wave expansion of the wave functions is used to ensure the convergence of the calculations. The structures are optimized until the Hellmann–Feynman forces are smaller than 1.0×10^{-3} eV Å^{-1}. The Brillouin zone (BZ) integration is carried out with a uniform $6 \times 6 \times 1$ k-grid. The MXene layer is separated from its periodic images by a 20 Å thick vacuum layer to minimize spurious interlayer interactions.

For the quasiparticle band structure calculations within the GW approximation,[18] we use a local version of the BERKELEYGW package[19] in which recently developed acceleration methods[24,25] are implemented. Normal conserving pseudopotentials[26] are used for all GW calculations, and all semicore subshells (*i.e.*, *n*s, *n*p, and *n*d semicore electrons, $n = 3$ for Ti, 4 for Zr, and 5 for Hf) are included as valence electrons. The Hybertsen–Louie generalized plasmon-pole model (HL-GPP)[18] is used to extend the static dielectric function to finite frequencies. Including semicore electrons and the use of norm-conserving potential require a rather high plane wave cutoff energy (175 Ry) and a large number of conduction bands have to be included in the GW calculations to ensure that the calculated results are fully converged.[24] In addition, GW calculations for 2D materials are known to converge extremely slowly[27–29] with respect to the density of 2D k-grid used in the BZ integration due to the analytical behavior of the 2D dielectric function and other relevant quantities as the wave vector q approaches 0. Recently, we have developed two methods[24,25] that aim directly at resolving these difficulties.

The first method[24] we developed replaces the cumbersome band-by-band summation in conventional GW calculations with a numerical integration in the energy space. Our method results in a speed-up factor of up to two orders of magnitude for large-scale GW calculations without sacrificing the accuracy. This method has been successfully applied to GW calculations for a wide range of materials.[24,30,31] The second method we developed[25] is specific for 2D GW calculations as we will discuss in more details later.

3. Results and discussion

3.1 Quasiparticle band structure of single layer Hf_2CO_2

Terminal oxygen can adsorb on either fcc or hcp sites. Previous studies have established that the fcc oxygen adsorption has the lowest energy.[13,14,32] In this work, we adopted the fcc geometry for O atoms. Single-layer Hf_2CO_2 MXene has a hexagonal structure consisting of five atomic layers as shown in Fig. 1. The optimized 2D hexagonal lattice constant is

3.265 Å, and the Hf–C and Hf–O bond lengths are 2.33 Å and 2.10 Å, respectively. Fig. 2 shows the PBE band structure superimposed with projections onto atomic orbitals. The valence band maximum (VBM) is placed at zero in Fig. 2. The lower group of valence states is mainly derived from O p states with some admixture of Hf d states, whereas the upper one has contributions from C p, Hf d, and O p states. The low energy conduction bands, on the other hand, consist mostly of Hf d states. The VBM states are located at the Γ point and are primarily composed of C p_x + p_y orbitals hybridized with O p_x + p_y and Hf d_{xz} + d_{yz}. The conduction band minimum (CBM) is located at the M point of the hexagonal BZ, consisting mostly of Hf d states. Since the CBM of Hf_2CO_2 MXene is derived from the Hf d states, it is expected that substituting Hf with isoelectronic transition metals with lower d-state energy will result in a reduced band gap as we will discuss later.

Fig. 3 compares the PBE and GW band structures of single-layer Hf_2CO_2. The PBE functional predicts an indirect band gap of 0.99 eV, to be compared with the GW band gap of 2.45 eV. The minimum direct band gap at the M point is about 3.60 eV within the GW approximation. The valence bandwidth is also significantly enhanced with the GW correction. With a moderate band gap of 2.45 eV and other promising properties[14] such as high thermal conductivity and carrier mobility, this MXene based 2D semiconductor holds great potential for future 2D electronics applications.

We now briefly discuss the convergence issue that is specific to GW calculations for 2D materials. In GW calculations, the BZ integration of the quasiparticle self-energy of state $|n\vec{k}>$ near the Γ ($\vec{q}=0$) point is carried out using a uniform k-grid (for 2D systems, an $N \times N \times 1$ grid), *i.e.*, $\Sigma_{n\vec{k}} = \sum_{\vec{q}} f_{\vec{q}} \Sigma(\vec{q})$. For bulk (3D) semiconductors, this summation converges quickly with increasing k-grid density. For example, for silicon (diamond structure with a 2-atom unit cell), a $6 \times 6 \times 6$ k-grid is sufficient to converge the calculated GW band gap to within 0.01 eV. For 2D materials, however, the convergence is extremely slow[27–29] due to the analytical behaviors of the 2D dielectric function and other relevant quantities as wave vector $\vec{q}$ approaches 0. Recently, we have successfully developed a combined subspace sampling and analytical integration technique[25] that can drastically reduce the required 2D k-grid sampling density for achieving fully converged GW results. Our method is inspired by a recent work[29] in which the authors proposed a nonuniform sampling scheme for GW calculations.

In our new method, the BZ integration of the self-energy of state $|n\vec{k}>$ near the Γ ($\vec{q}=0$) point is replaced with an analyti-

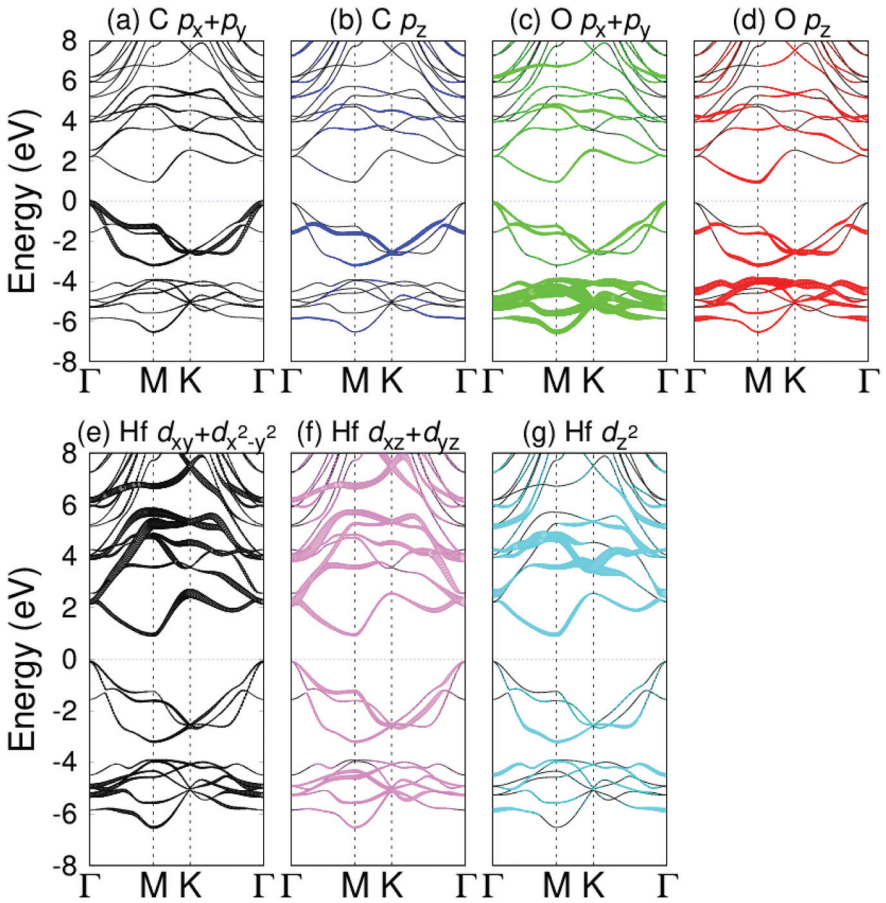

Fig. 2 Atomic-orbital projected band structure of single-layer Hf_2CO_2 calculated using the PBE functional.

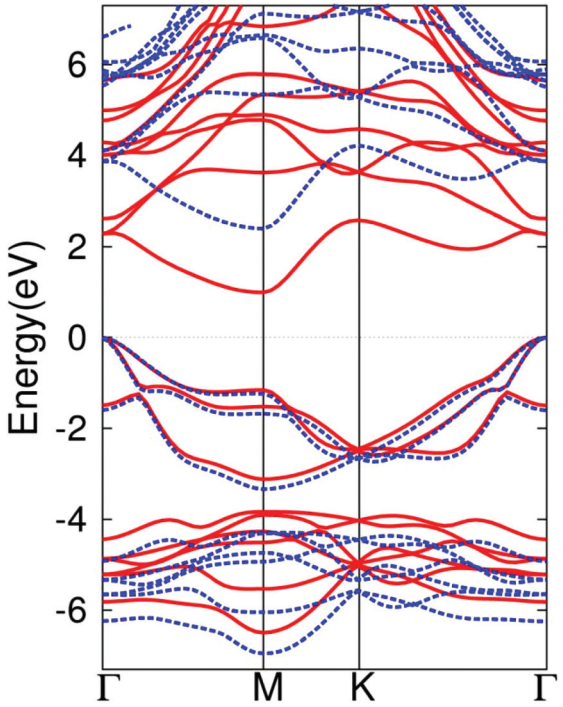

Fig. 3 DFT-PBE (red) and GW (dotted blue) band structures of single-layer Hf_2CO_2.

cal integration over the mini-BZ (mBZ) enclosing the Γ point, *i.e.*, $\Sigma_{n\vec{k}} = \sum_{\vec{q}\neq 0} f_{\vec{q}}\Sigma(\vec{q}) + \frac{f_0}{V_{mBZ}}\int_{mBZ}\Sigma(\vec{q})d\vec{q}$. We first calculate $\Sigma(\vec{q})$ for a few small q-points within the mini-BZ as shown with blue dots in Fig. 4. These results are then used to fit $\Sigma(\vec{q})$ with some analytical form as shown in Fig. 4 with the blue curve. Analytical integration within the mBZ is then carried out using this function. To illustrate the accuracy of the fitting function, we have also plotted in Fig. 4 $\Sigma(\vec{q})$ calculated at other q-points

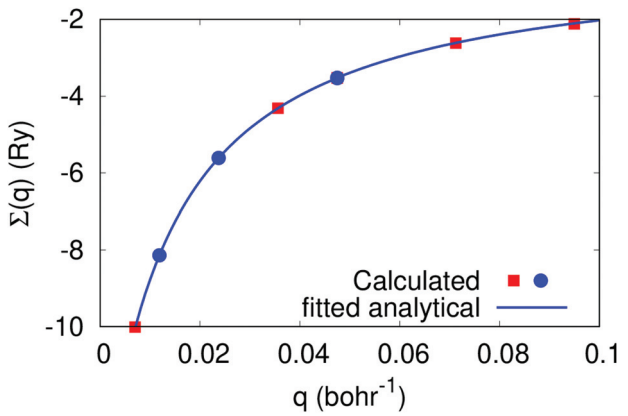

Fig. 4 Fitting the self-energy contribution from the mBZ enclosing the Γ point with an analytical function for subsequent integration. Blue dots are the data points used to fit the function (shown with the blue curve). Red squares are additional data points to show the quality of the fitting function.

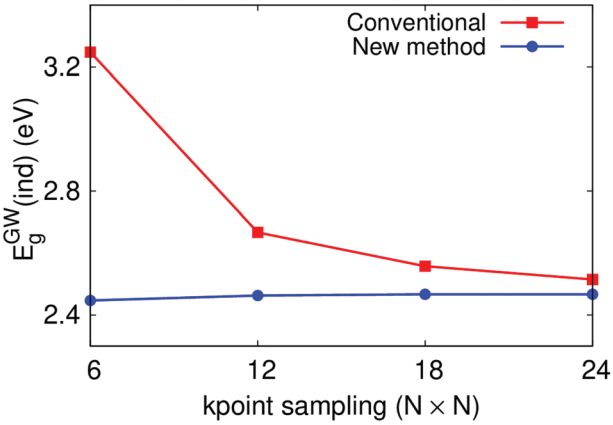

Fig. 5 Calculated GW band gap of single-layer Hf_2CO_2 as a function of k-point sampling density: comparison between the conventional uniform sampling scheme and the newly developed method.

(red squares), showing excellent agreement between the calculated results and the fitting function.

Using this method, we are able to carry out converged GW calculations for 2D materials using a 6 × 6 × 1 coarse k-grid as shown in Fig. 5 in which we compare the performance of our new method with the conventional uniform k-point sampling approach. Using our new method, the calculated band gap converges to within 0.02 eV with a very coarse k-grid of 6 × 6 × 1. In comparison, the band gap does not seem to converge even with a very fine 24 × 24 × 1 grid using the conventional method. Note that the convergence behavior of the GW results calculated using the uniform sampling approach shown in Fig. 5 is consistent with previous work. For example, it has been shown that a k-grid of at least 24 × 24 × 1 is need to properly converged the GW band gap of MoS_2.[33] Considering the fact that the computational cost of GW calculations (the calculation of the electron polarizability) scales as $O(N_k^2)$ where N_k is the number of k-points used to sample the BZ, our method represents a speed-up factor of over two orders of magnitude compared with the conventional method. Combining this method with another method[24] we developed in which the conventional band-by-band summation in the GW calculations is replaced with an energy integration, we can now carry out fully converged GW calculations for 2D materials with a speed-up factor of about three orders of magnitude.

3.2 M_2CO_2 (M = Hf, Zr, and Ti): structural and electronic properties

We now investigate the possibility of tuning the band gap of M_2CO_2 MXene based 2D semiconductors. As we have shown in Fig. 2, the CBM state of Hf_2CO_2 is mainly derived from Hf d states. Therefore, it is plausible the band gap of Hf_2CO_2 can be tuned by replacing Hf with isoelectronic transition metals such as Ti or Zr. In particular, since the 3d level of Ti atom is significantly lower than the Hf 5d level, replacing Hf with Ti may result in significantly lowered CBM thus reducing the band gap. In addition, due to their chemical similarity, it is

expected that semiconductor alloys of M_2CO_2 (M = Hf, Zr, and Ti) can be synthesized, providing a MXene based 2D material system with tunable band gap.

Before investigating their electronic structures, we first evaluate the stability of M_2CO_2 (M = Hf, Zr, and Ti) by calculating their formation energies. We define the formation energy as the difference in total energy between single-layer M_2CO_2 and stable competing subsystems, *i.e.*, solid metal and CO_2 gas molecules, i.e, $\Delta E = E(M_2CO_2) - [E(\text{metal}) + E(CO_2)]$. Table 1 shows the calculated formation energies and lattice constants for the four single layer MXenes. Although the formation energy (absolute value) of Ti_2CO_2 is smaller than that of Hf_2CO_2, a formation energy of −6.67 eV per formula unit (f.u.) still suggests that Ti_2CO_2 is thermodynamically stable and synthetically viable.

Table 1 Formation energies (eV/f.u.), lattice constants (Å) and band gaps (eV) of single-layer Hf_2CO_2, Zr_2CO_2, Ti_2CO_2 and (HfTi)CO_2 MXene semiconductors

	Hf_2CO_2	Zr_2CO_2	Ti_2CO_2	(HfTi)CO_2
Formation energy	−8.17	−7.28	−6.67	−7.20
Lattice constant	3.265	3.322	3.034	3.161
DFT-PBE gap	0.99	0.88	0.26	0.55
HSE gap	1.59	1.45	0.90	1.28
GW gap	2.45	2.13	1.15	1.80

Fig. 6 shows the DFT-PBE band structures of Zr_2CO_2 and Ti_2CO_2. The DFT-PBE band gap of Ti_2CO_2 (0.26 eV) is indeed much smaller than that of Hf_2CO_2 as expected. Replacing Hf with Zr, however, does not lead to significant changes to the band structure. The PBE band gap of Zr_2CO_2 is about 0.88 eV, which is only 0.1 eV smaller than that of Hf_2CO_2 as shown in Table 1. This is because 4d and 5d transition metals

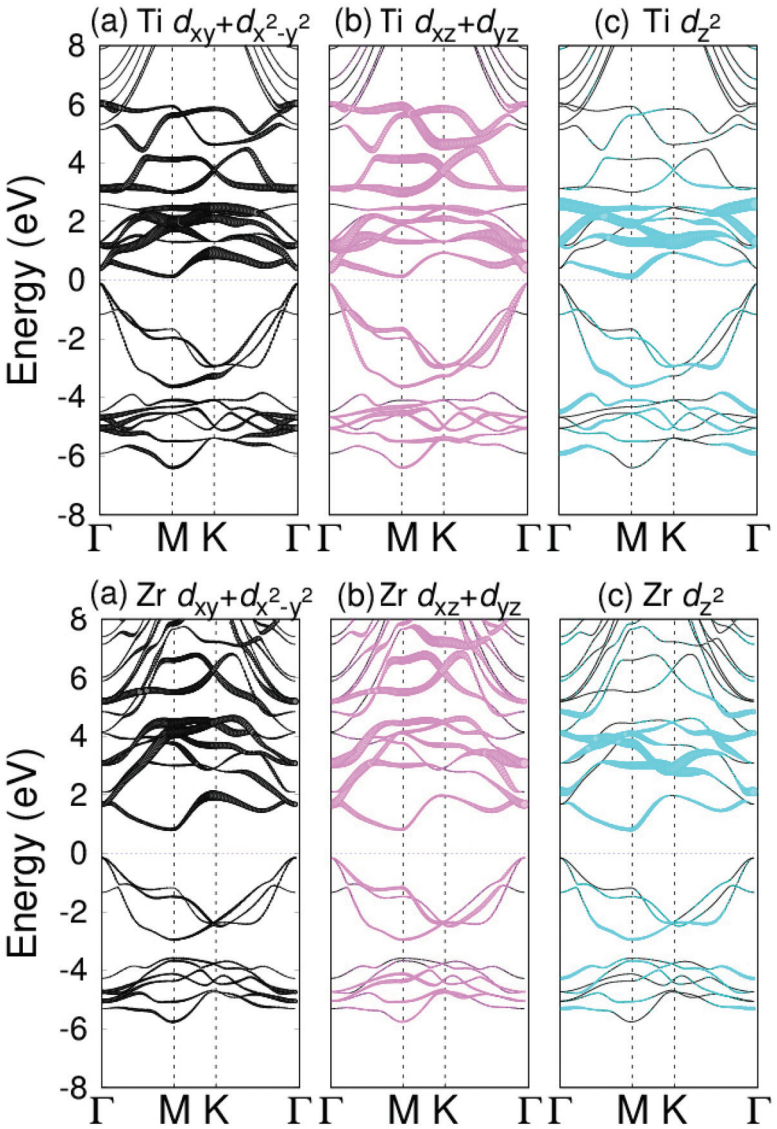

Fig. 6 Atomic-orbital projected band structure of single-layer Ti_2CO_2 (upper) and Zr_2CO_2 (lower) calculated using the PBE functional.

share similar physical properties such as d level positions and atomic radii. Zr_2CO_2 has the largest lattice constant among the three systems. This is expected since Zr has the greatest ionic radius. We have also carried out GW calculations for the band gap of Zr_2CO_2 and Ti_2CO_2. Including GW self-energy corrections increases the band gap of Ti_2CO_2 to 1.15 eV and that of Zr_2CO_2 to 2.13 eV. These results suggest an interesting possibility of continuously tuning the band gap of these 2D semiconductors from 2.45 to 1.15 eV through alloying.

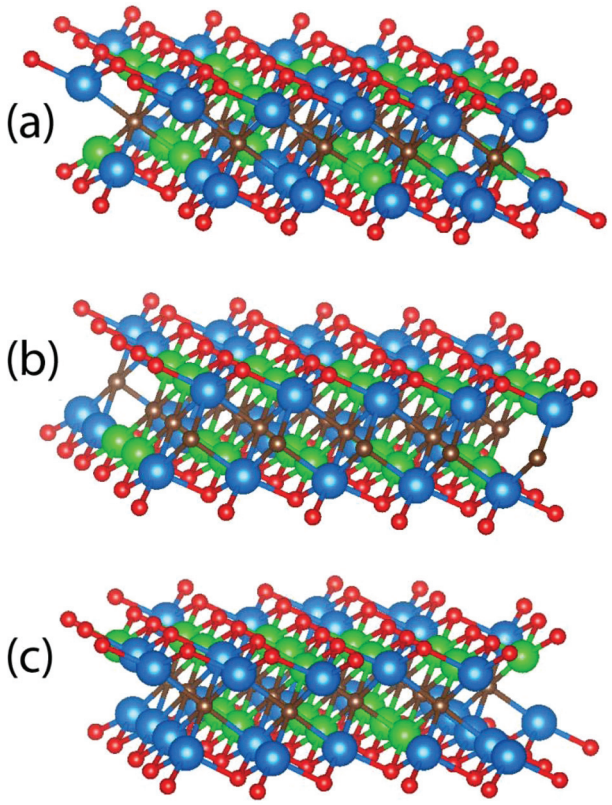

Fig. 7 A few structural models for the $HfTiCO_2$ 2D random alloy used in this work.

3.3 Continuous band gap tuning of $Hf_{2-x}Ti_xCO_2$ 2D semiconductor alloys

Isoelectronic substitution minimally disturbs the chemical bonding of a material while offering the possibility of significantly modifying the low-energy (near-edge) electronic states. The quasiparticle band gap of Hf_2CO_2 is predicted to be 2.45 eV whereas that of Ti_2CO_2 is about 1.15 eV. Therefore, alloying Hf_2CO_2 with Ti_2CO_2 may provide a material system with a widely tunable band gap. To this end, we have calculated the electronic properties of $Hf_{2-2x}Ti_{2x}CO_2$ ($0 \leq x \leq 1$) alloys. We create a $4 \times 4 \times 1$ supercell containing 80 atoms for studying the alloy systems. Except for the end systems, for each Ti concentration x, several inequivalent structures are randomly created and their structures are fully optimized.

Fig. 7 shows a few structural models that we created for the $HfTiCO_2$ random alloy. We mention the special quasirandom structure (SQS) approach[34] is a well-established approach for generating finite structural models that best mimic the radial correlation functions of perfectly random structures, and ideally one should adopt this approach for creating structural models for random alloys. Since we find that the calculated band gap does not depend sensitively on the specific structures (with a variation of about ±0.1 eV), we did not attempt to create SQS for these random alloys.

On the other hand, we have noticed that Wong and collaborators[32] recently carried out a detailed study on the structural and thermodynamic properties of these random alloys. They concluded that $Ti_{2(1-x)}Zr_{2x}CO_2$, $Ti_{2(1-x)}Hf_{2x}CO_2$, and $Zr_{2(1-x)}Hf_{2x}CO_2$ exist as disordered solid solutions. These results are expected since isoelectronic ions usually mix rather well as they have the same valency, especially when their ionic radii do not differ significantly as suggested by Hume–Rothery rules. Other MXene alloys have also been investigated theoretically.[35] Admittedly, the stability of a material shall be ultimately determined by experiments. In recent years, experimentalists have been very successfully (and sometimes unexpectedly) in synthesizing metastable compounds. In particular, chemical vapor deposition (CVD) has been shown to be a powerful method for synthesizing 2D materials and heterostructures.[36]

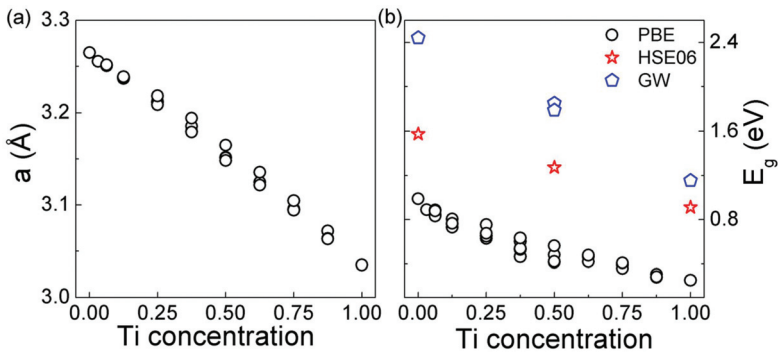

Fig. 8 Lattice constant (left) and band gap (right) of single-layer $Hf_{2-2x}Ti_{2x}CO_2$ alloy as functions of Ti concentration x. The band gaps are calculated within the DFT-PBE approach for all Ti concentrations and using the HSE and GW approaches for selected concentrations.

Fig. 8(a) shows that the lattice constant of $Hf_{2-2x}Ti_{2x}CO_2$ semiconductor alloy varies nearly linearly with Ti concentration x, obeying Vegard's law. Interestingly, the calculated DFT-PBE band gap of $Hf_{2-2x}Ti_{2x}CO_2$ as a function of Ti concentration also shows a nearly linear dependence [Fig. 8(b)], suggesting a very small band gap bowing parameter for this system. For a given Ti concentration, different structures show slightly different band gap with a deviation of ±0.1 eV from their averaged values. The HSE and GW results for three Ti concentrations are also shown in Fig. 8(b) for comparison. Our results suggest that the quasiparticle band gap of $Hf_{2-2x}Ti_{2x}CO_2$ alloy can be continuously tuned from 2.45 eV to 1.15 eV.

Isoelectronic substitutions may be achieved beyond single pair of elements. Since the band gap of Zr_2CO_2 is just slightly smaller than that of Hf_2CO_2, alloys of these two semiconductors may not offer significant band gap tunability. However, considering the fact that Zr_2CO_2 has a larger lattice constant than Hf_2CO_2, whereas Ti_2CO_2 has the smallest lattice constant, it may be beneficial to synthesize ternary alloys $Hf_{2-2x-2y}Zr_{2x}Ti_{2y}CO_2$ to minimize the lattice strain. In addition, co-doping with d^1 and d^3 pairs (*e.g.*, Y and Nb, or Sc and Ta) may also be considered. We would like to mention that mechanical strain can also be used to tune the band gap of semiconductors. For example, we find that the band gap of Hf_2CO_2 reduces at a rate of about 0.1 eV per 1% compressive 2D lattice strain. It may be desirable to combine mechanical strain with chemical substitution to realize wide band gap tunability in certain applications.

4. Summary

M_2CO_2 (M = Hf, Zr, and Ti) MXene based tunable band gap 2D semiconductors are investigated using DFT and GW approaches. Recently developed accelerated GW methods are employed in this study. The quasiparticle band gap of single-layer Hf_2CO_2 is predicted to be 2.45 eV, which is significantly different from about 1.59 eV predicted using the HSE functional, suggesting the importance of accurate quasiparticle calculations for predicting the electronic properties of 2D semiconductors. The conduction bands of Hf_2CO_2 are mainly derived from Hf d states. This points to the possibility of tuning the band gap through Ti substitutions of Hf since Ti has lower d levels. Indeed, the calculated quasiparticle band gap of Ti_2CO_2 is about 1.15 eV, and we show that the quasiparticle band gap of $Hf_{2-2x}Ti_{2x}CO_2$ ($0 \leq x \leq 1$) semiconductor alloy can be continuously tuned from 2.45 to 1.15 eV. Introducing Zr into the alloy system is expected to reduce the lattice strain while leaving the fundamental gap nearly unchanged. We believe that M_2CO_2 MXene based semiconductors and their alloys, which combine advantages such as structural stability, chemical flexibility, and electronic tunability, offer a unique material for future 2D electronics applications.

Conflicts of interest

There are no conflicts to declare.

Acknowledgements

This work was supported in part by the National Natural Science Foundation of China (No. 11875004, 11505006, and 11628407) and Beijing Natural Science Foundation (Grant No. 2182042). Work at UB was supported by the US NSF (DMR-1506669 and DMREF-1626967). We acknowledge the computational support provided by the Center for Computational Research at the University at Buffalo, SUNY and the Beijing Computational Science Research Center.

References

1 B. Anasori, M. R. Lukatskaya and Y. Gogotsi, 2D Metal Carbides and Nitrides (MXenes) for Energy Storage, *Nat. Rev. Mater.*, 2017, **2**, 16098.
2 M. Naguib, M. Kurtoglu, V. Presser, J. Lu, J. Niu, M. Heon, L. Hultman, Y. Gogotsi and M. W. Barsoum, Two-Dimensional Nanocrystals Produced by Exfoliation of Ti3AlC2, *Adv. Mater.*, 2011, **23**(37), 4248–4253.
3 M. Naguib, O. Mashtalir, J. Carle, V. Presser, J. Lu, L. Hultman, Y. Gogotsi and M. W. Barsoum, Two-Dimensional Transition Metal Carbides, *ACS Nano*, 2012, **6**(2), 1322–1331.
4 M. Naguib, V. N. Mochalin, M. W. Barsoum and Y. Gogotsi, 25Th Anniversary Article: MXenes: A New Family of Two-Dimensional Materials, *Adv. Mater.*, 2014, **26**(7), 992–1005.
5 M. W. Barsoum, *MAX Phases: Properties of Machinable Ternary Carbides and Nitrides*, John Wiley & Sons, 2013.
6 Y. Xie, M. Naguib, V. N. Mochalin, M. W. Barsoum, Y. Gogotsi, X. Yu, K. Nam, X. Yang, A. I. Kolesnikov and P. R. Kent, Role of Surface Structure On Li-ion Energy Storage Capacity of Two-Dimensional Transition-Metal Carbides, *J. Am. Chem. Soc.*, 2014, **136**(17), 6385–6394.
7 J. Hu, B. Xu, C. Ouyang, S. A. Yang and Y. Yao, Investigations On V2C and V2CX2 (X = F, OH) Monolayer as a Promising Anode Material for Li Ion Batteries From First-Principles Calculations, *J. Phys. Chem. C*, 2014, **118**(42), 24274–24281.
8 Q. Tang, Z. Zhou and P. Shen, Are MXenes Promising Anode Materials for Li Ion Batteries? Computational Studies On Electronic Properties and Li Storage Capability of Ti3C2 and Ti3C2X2 (X = F, OH) Monolayer, *J. Am. Chem. Soc.*, 2012, **134**(40), 16909–16916.
9 A. D. Dillon, M. J. Ghidiu, A. L. Krick, J. Griggs, S. J. May, Y. Gogotsi, M. W. Barsoum and A. T. Fafarman, Highly Conductive Optical Quality Solution-Processed Films of 2D Titanium Carbide, *Adv. Funct. Mater.*, 2016, **26**(23), 4162–4168.
10 M. R. Lukatskaya, O. Mashtalir, C. E. Ren, Y. Dall Agnese, P. Rozier, P. L. Taberna, M. Naguib, P. Simon,

M. W. Barsoum and Y. Gogotsi, Cation Intercalation and High Volumetric Capacitance of Two-Dimensional Titanium Carbide, *Science*, 2013, **341**(6153), 1502–1505.

11 Q. Hu, D. Sun, Q. Wu, H. Wang, L. Wang, B. Liu, A. Zhou and J. He, MXene: A New Family of Promising Hydrogen Storage Medium, *J. Phys. Chem. A*, 2013, **117**(51), 14253–14260.

12 X. Zhang, Z. Ma, X. Zhao, Q. Tang and Z. Zhou, Computational Studies On Structural and Electronic Properties of Functionalized MXene Monolayers and Nanotubes, *J. Mater. Chem. A*, 2015, **3**(9), 4960–4966.

13 M. Khazaei, M. Arai, T. Sasaki, C. Y. Chung, N. S. Venkataramanan, M. Estili, Y. Sakka and Y. Kawazoe, Novel Electronic and Magnetic Properties of Two-Dimensional Transition Metal Carbides and Nitrides, *Adv. Funct. Mater.*, 2013, **23**(17), 2185–2192.

14 X. Zha, Q. Huang, J. He, H. He, J. Zhai, J. S. Francisco and S. Du, The Thermal and Electrical Properties of the Promising Semiconductor MXene Hf_2CO_2, *Sci. Rep.*, 2016, **6**, 27971.

15 J. Heyd, G. E. Scuseria and M. Ernzerhof, Hybrid Functionals Based On a Screened Coulomb Potential, *J. Chem. Phys.*, 2003, **118**(18), 8207–8215.

16 J. Heyd, G. E. Scuseria and M. Ernzerhof, Erratum: 'Hybrid Functionals Based On a Screened Coulomb Potential', *J. Chem. Phys.*, 2006, **124**(21), 219906 [*J. Chem. Phys.*, 2003, **118**, 8207].

17 A. Ennaoui, S. Fiechter, C. Pettenkofer, N. Alonso-Vante, K. Büker, M. Bronold, C. Höpfner and H. Tributsch, Iron Disulfide for Solar Energy Conversion, *Sol. Energy Mater. Sol. Cells*, 1993, **29**(4), 289–370.

18 M. S. Hybertsen and S. G. Louie, Electron Correlation in Semiconductors and Insulators: Band Gaps and Quasiparticle Energies, *Phys. Rev. B: Condens. Matter Mater. Phys.*, 1986, **34**(8), 5390–5413.

19 J. Deslippe, G. Samsonidze, D. A. Strubbe, M. Jain, M. L. Cohen, S. G. Louie and G. W. Berkeley, A Massively Parallel Computer Package for the Calculation of the Quasiparticle and Optical Properties of Materials and Nanostructures, *Comput. Phys. Commun.*, 2012, **183**(6), 1269–1289.

20 G. Kresse and J. Furthmüller, Efficiency of *Ab initio* Total Energy Calculations for Metals and Semiconductors Using a Plane-Wave Basis Set, *Comput. Mater. Sci.*, 1996, **6**(1), 15–50.

21 P. E. Blöchl, Projector Augmented-Wave Method, *Phys. Rev. B: Condens. Matter Mater. Phys.*, 1994, **50**(24), 17953–17979.

22 J. P. Perdew and W. Yue, Accurate and Simple Density Functional for the Electronic Exchange Energy: Generalized Gradient Approximation, *Phys. Rev. B: Condens. Matter Mater. Phys.*, 1986, **33**(12), 8800–8802.

23 J. P. Perdew, K. Burke and M. Ernzerhof, Generalized Gradient Approximation Made Simple, *Phys. Rev. Lett.*, 1996, **77**(18), 3865.

24 W. Gao, W. Xia, X. Gao and P. Zhang, Speeding up GW Calculations to Meet the Challenge of Large Scale Quasiparticle Predictions, *Sci. Rep.*, 2016, **6**, 36849.

25 Y. Wu, W. Xia, W. Gao, F. Jia, P. Zhang and W. Ren, Quasiparticle Electronic Structure of Honeycomb C3N: From Monolayer to Bulk, *2D Mater.*, 2019, **6**(1), 015018.

26 N. Troullier and J. L. Martins, Efficient Pseudopotentials for Plane-Wave Calculations, *Phys. Rev. B: Condens. Matter Mater. Phys.*, 1991, **43**(3), 1993–2006.

27 D. Y. Qiu, F. H. Da Jornada and S. G. Louie, Optical Spectrum of MoS2: Many-Body Effects and Diversity of Exciton States, *Phys. Rev. Lett.*, 2013, **111**(21), 216805.

28 F. Hüser, T. Olsen and K. S. Thygesen, How Dielectric Screening in Two-Dimensional Crystals Affects the Convergence of Excited-State Calculations: Monolayer MoS2, *Phys. Rev. B: Condens. Matter Mater. Phys.*, 2013, **88**(24), 245309.

29 F. H. Da Jornada, D. Y. Qiu and S. G. Louie, Nonuniform Sampling Schemes of the Brillouin Zone for Many-Electron Perturbation-Theory Calculations in Reduced Dimensionality, *Phys. Rev. B*, 2017, **95**(3), 035109.

30 Y. Wu, W. Xia, W. Gao, W. Ren and P. Zhang, Engineering the Near-Edge Electronic Structure of SnSe through Strains, *Phys. Rev. Appl.*, 2017, **8**(3), 034007.

31 W. Gao, W. Xia, Y. Wu, W. Ren, X. Gao and P. Zhang, Quasiparticle Band Structures of CuCl, CuBr, AgCl, and AgBr: The Extreme Case, *Phys. Rev. B*, 2018, **98**(4), 045108.

32 Z. M. Wong, T. L. Tan, S. W. Yang and G. Q. Xu, Enhancing the Photocatalytic Performance of MXenes via Stoichiometry Engineering of Their Electronic and Optical Properties, *ACS Appl. Mater. Interfaces*, 2018, **10**(46), 39879.

33 D. Y. Qiu, F. H. Da Jornada and S. G. Louie, Screening and Many-Body Effects in Two-Dimensional Crystals: Monolayer MoS2, *Phys. Rev. B*, 2016, **93**(23), 235435.

34 A. Zunger, S. H. Wei, L. G. Ferreira and J. E. Bernard, Special Quasirandom Structures, *Phys. Rev. Lett.*, 1990, **65**(3), 353.

35 T. L. Tan, H. M. Jin, M. B. Sullivant, B. Anasori and Y. Gogotsi, High-Throughput Survey of Ordering Configurations in MXene Alloys Across Compositions and Temperatures, *ACS Nano*, 2017, **11**(5), 4407.

36 Z. Cai, B. Liu, X. Zou and H. M. Cheng, Chemical Vapor Deposition Growth and Applications of Two-Dimensional Materials and Their Heterostructures, *Chem. Rev.*, 2018, **118**(13), 6091.

